Energy 261 (2022) 125275

Contents lists available at ScienceDirect

Energy

journal homepage: www.elsevier.com/locate/energy

Domestic hot water production system in a hospital: Energy audit and evaluation of measures to boost the solar contribution

Antonio Atienza-Márquez *, Fernando Domínguez Muñoz, Francisco Fernández Hernández, José Manuel Cejudo López

Universidad de Málaga, Department of Mechanical, Thermal and Fluids Engineering, Energy Research Group (GEUMA), C/Arquitecto Francisco Peñalosa 6, 29010, Málaga, Spain

ARTICLE INFO

Keywords:
Hospital building
Domestic hot water (DHW)
Solar thermal
Energy audit
Energy retrofit
Techno-economic analysis

ABSTRACT

Hospitals consume large quantities of energy to produce hot water and offset the distribution and recirculation thermal losses. This paper analyses a solar thermal system combined with gas boilers for domestic hot water production in a medium-size hospital. The solar contribution to the total demand (27%) is below design expectations (75%), resulting in significant gas consumption. The energy audit conducted in the first part of the paper highlights the vast thermal loss through poorly insulated pipes as the primary cause of the poor solar fraction. This issue is endemic to hot water-intensive buildings. The second part of the paper addresses the techno-economic evaluation of energy retrofit measures to reach a solar fraction of 60%. The simulation results indicate that cost-optimised solutions generally expand the solar caption area by 43–57% and improve insulations to reduce thermal losses by 70%. Depending on carbon taxes, the cost of hot water production would be 31–41 cent-€/kWh, which represents a 15–45% reduction from the current costs. Under stringent climate policies, installing heat pumps may further enhance economic competitiveness. The indicators and charts developed in this work are helpful decision-making tools concerning the energy refurbishment of solar domestic hot water systems.

1. Introduction

The building sector represents one-third of the global final energy consumption [1]. Boosting its energy efficiency is thus an essential step to cope with climate change, a code red for humanity [2]. During the last decade, engineers and architects have been developing projects to achieve the "nearly zero energy building" (NZEB) target [3], both in existing and new buildings [4]. Although this concept is full of nuances [5], the fundamentals are to reduce the energy demand, carbon footprint, and utility bills while maintaining occupants' comfort and satisfying the energy demand mainly through renewable sources [6].

The literature dealing with energy efficiency in buildings is extensive. Researchers have proposed innovative designs or energy retrofit packages for different building typologies [7]; for example: residential buildings [8], offices [9], schools [10], hotels [11], and hospitals [12], to cite just a few examples. Hospitals have received much attention because of their intensive energy consumption and strict reliability requirements. According to González et al. [13], hospitals account for 7% of the energy consumption of the tertiary sector buildings in Spain. In the United States, hospitals represent 10% of the energy consumption of the commercial sector [14]. A number of researchers have performed energy audits in existing hospitals, either public [15] or private [16], to identify energy conservation opportunities and propose measures to minimise energy consumption and greenhouse gas (GHG) emissions [17].

Research on energy consumption in hospitals has tended to focus on HVAC systems [18] because they account for a significant fraction of the total energy consumption [12] and are a determinant element in controlling the indoor environmental quality [19]. In contrast, little research has been conducted on other energy uses that, while providing essential services, usually have a lower impact on the energy indicators of the building. An important example is the domestic hot water (DHW) preparation system, which in Spain accounts for around 8% of the primary energy consumption in hospitals [20].

Hospitals are large DHW consumers for uses such as patient hygiene, cleaning, and kitchen services [21]. Water heating represents a major source of GHG emissions because hot water is typically prepared in

* Corresponding author.
E-mail address: atienza-marquez@uma.es (A. Atienza-Márquez).

https://doi.org/10.1016/j.energy.2022.125275
Received 28 January 2022; Received in revised form 12 July 2022; Accepted 23 August 2022
Available online 5 September 2022

Nomenclature

Abbreviations

BAU	Business as usual scenario
DHW	Domestic hot water
GHG	Greenhouse gases
SDS	Sustainable development scenario
W1⋯W7	Hot water state points
ZES	Zero emissions scenario

Variables

A	Heat transfer area, m^2
AE	Annual expenses, €
C	Cost, €
COP	Coefficient of performance
Cp	Specific heat, kJ/(kg·K)
D	Hot water demand, m^3/h, or Diameter, m
EER	Energy efficiency ratio, W/W
EF	GHG emissions factor, kg-$CO_{2,eq}$/MWh
FCI	Fixed capital investment, €
HHV	Higher heating value, kWh/m^3
k	Thermal conductivity, W/m
L	Length, m
$LCoHW$	Levelised cost of hot water, €/kWh
LHV	Lower heating value, kWh/m^3
$\dot{m}$	Mass flow rate, kg/s
n	System lifespan, years
$NMBE$	Normalized mean bias error, %
OAE	Other annual expenses, €
OFC	Other fixed costs, €
PEC	Purchased equipment cost, €
$\dot{Q}$	Heat flow, kW
r	Annual discount rate
$RMSE$	Root mean square error, %
SF	Solar fraction, %
T	Temperature, K
TCI	Total capital investment, €
U	Overall heat transfer coefficient, W/(m^2·K), or internal energy, kJ/(kg·K)
V	Volume (gas or water) consumed, m^3
$\dot{V}$	Volumetric flow rate, m^3/s
$\dot{W}$	Power, kW

Greek letters

α	Baseload hot water consumption
β	Hourly variation coefficient
η	Efficiency, %
γ	Seasonal variation coefficient

Subscripts

AC	Air-conditioning
b	Boiler
C	Compressor
e	Emissions
el	Electricity
eq	Equivalent
exp	Experimental
G	Natural gas
HP	Heat pump
is	Thermal insulation material
L	Thermal losses
o	Outer
P	Pump
r	Rated
sim	simulation
SOLAR	Solar
tot	Total
w	Water

centralized systems that burn fossil fuels (e.g., gas-fired boilers [22]). Despite numerous barriers that hamper energy efficiency in hospital buildings [23], a widespread practice to improve environmental efficiency consists of meeting a fraction of hot water demands with solar thermal collectors. For example, Sánchez-Barroso et al. [24] analysed the energy, economic and environmental savings that could be achieved by installing solar thermal collectors under different solar fraction scenarios to produce DHW in a group of hospitals in Spain. Besides, recent European Union-funded projects such as SophiA [26] aim to integrate solar thermal systems in hospitals in Africa to provide sustainable off-grid energy supply.

However, the solar fraction of operating systems often underperforms relative to designs based on simulation results (e.g., using TRNSYS [25], EnergyPlus [26] or T*SOL [27]). This issue was observed, for example, by Meister and Beausoleil-Morrison [28] in the solar thermal system installed in a research house. These problems are critical in buildings with intensive DHW demand, such as hospitals, to the authors' knowledge. Therefore, fossil fuel consumption and GHG emissions may exceed those predicted at the design stage.

These performance deviations could be due to failed designs (which, as shown in Carretero-Ayuso et al. [29], are common concerning the envelope of hospitals) and/or poor project executions. For example, inadequate insulation of pipes may affect the energy losses of DHW systems and reduce the solar fraction. In fact, these thermal losses account for an important part of the energy consumption of the DHW systems in buildings. Hamburg et al. studied this issue in residential buildings [30]. Cholewa et al. [31] analysed the long-term monitoring data gathered from the DHW preparation systems in several multifamily buildings and thermal substations to assess the share of thermal losses to the total energy consumption and propose energy efficiency methods. However, in the open literature dealing with energy efficiency in hospitals, there is a lack of actual performance data (e.g., energy consumption) on DWH preparation systems.

This paper presents the detailed energy audit of a solar-assisted DHW system in a medium-size hospital, identifying a set of factors that deteriorate the performance of the solar thermal subsystem. The problems pointed out are poorly documented in the open literature and are probably of common occurrence in numerous DHW intensive buildings.

The structure of the paper is as follows. After the introduction, Section 2 presents the case study DHW system, the simulation model, and the techno-economic indicators used to assess the system's performance. Section 3 presents the results of the long-term monitoring of the system and the calibration of the modelling. The techno-economic evaluation of energy retrofit measures to boost the solar fraction is also tackled in this section. The indicators and graphic tools developed in this study allow speeding up the decision-making process on the most suitable energy retrofit measures for DHW systems, thereby encouraging energy conservation efforts in hot-water intensive buildings.

2. Description and modelling of the case-study hospital's hot water system

2.1. Description and operation

The so-called "Hospital Comarcal de la Axarquía", selected as a case-study for long-term monitoring, is located in Vélez-Málaga (36.75°N,

−4.09°W), a small city in southern Spain. It is a public medium-size healthcare building (four floors, 193 beds, and a total surface of 22,379 m^2) with DHW demand throughout the whole year. Fig. 1 shows pictures of the external façade and partial views of the solar field installed on the building's roof. The energy needs of the hospital itself could be considered a polygeneration system since it is integrated by different energy systems (e.g., PV installation, absorption machine, cogeneration engine).

This paper focuses on the hospital's DHW preparation and distribution system, whose schematic layout is shown in Fig. 2. The installation is divided into (1) the solar thermal system, (2) the auxiliary system and (3) the hot water distribution network. The solar collector has a net caption area of 180.14 m^2. It consists of three parallel-connected arrays of seven large-format collectors each. Each array is sub-divided into four parallel-connected subarrays. Three of them consist of 2 row-connected collectors. The other subarray consists of a single collector. The auxiliary system is a 440-kW gas-fired boiler that supplies hot water at 90 °C to a water treatment device (so-called "pasteuriser") where DHW is superheated for a sufficient time to prevent legionella growth. The system operates round-the-clock and with a steady recirculation flow rate. Therefore, hot tap water is available at the consumption points with no waiting times.

The system operates as follows. The water stream S1 leaving the solar field enters the heat exchanger HE-1, where the water stream A1 pumped from the bottom of the solar storage tank ST1 is heated up. Then, stream A2 is discharged at the top of the tank to promote thermal stratification. The primary fluid stream S2 leaving the heat exchanger HE-1 is still at a high temperature, so it is used in heat exchanger HE-2 to preheat the mains water stream W1. The water leaving the heat exchanger HE-2 (stream W2) enters the service tank where it is mixed with the recirculation stream W7 and with the water stream W3 that has absorbed the heat from the solar storage circuit through the heat exchanger HE-3. Afterward, the hot water stream W6 leaves the pasteuriser at 60 °C and reaches the taps on each building floor through the pipe network.

The control system is vital for the energy management of the installation. The following algorithms are applied to the pumps of the system:

- *Pump P1* (primary solar circuit): It will activate when the radiation level on the caption plane is above 185 W/m^2 and turned off when it falls below 160 W/m^2. Additionally, the controller of the pump P1 is equipped with a frequency variator to control the flow rate. The pumping capacity is 100% (i.e., 50 Hz) when the temperature of the stream W1 reaches 87 °C, while it is reduced proportionally down to 50% (i.e., 25 Hz) of the nameplate value if that temperature falls below 50 °C.
- *Pump P2* (solar storage, i.e., secondary circuit): It will activate whether the temperature of the stream W1 leaving the solar collectors is at least 1.5 °C higher than the temperature at the upper level of the solar storage tank and with and on/off performance (hysteresis of 0.5 °C) and without flow regulation.
- *Pump P3* (thermal discharging from solar storage circuit): It will activate when the temperature at the upper level of the solar storage tank is at least 5 °C higher than the temperature of the service tank at its bottoming level. The pump switches off whether that temperature difference drops below 1 °C.
- *Pump P4*: It follows the same control logic as the pump P3, but is equipped with a frequency shifter that regulates the flow rate. The control signal varies proportionally between 50% and 100% (i.e., from 25 to 50 Hz). The flow rate corresponds to the nameplate capacity if the temperature difference between streams W3 and W4 in the heat exchanger HE-3 is 5 °C or higher. The flow rate is reduced to

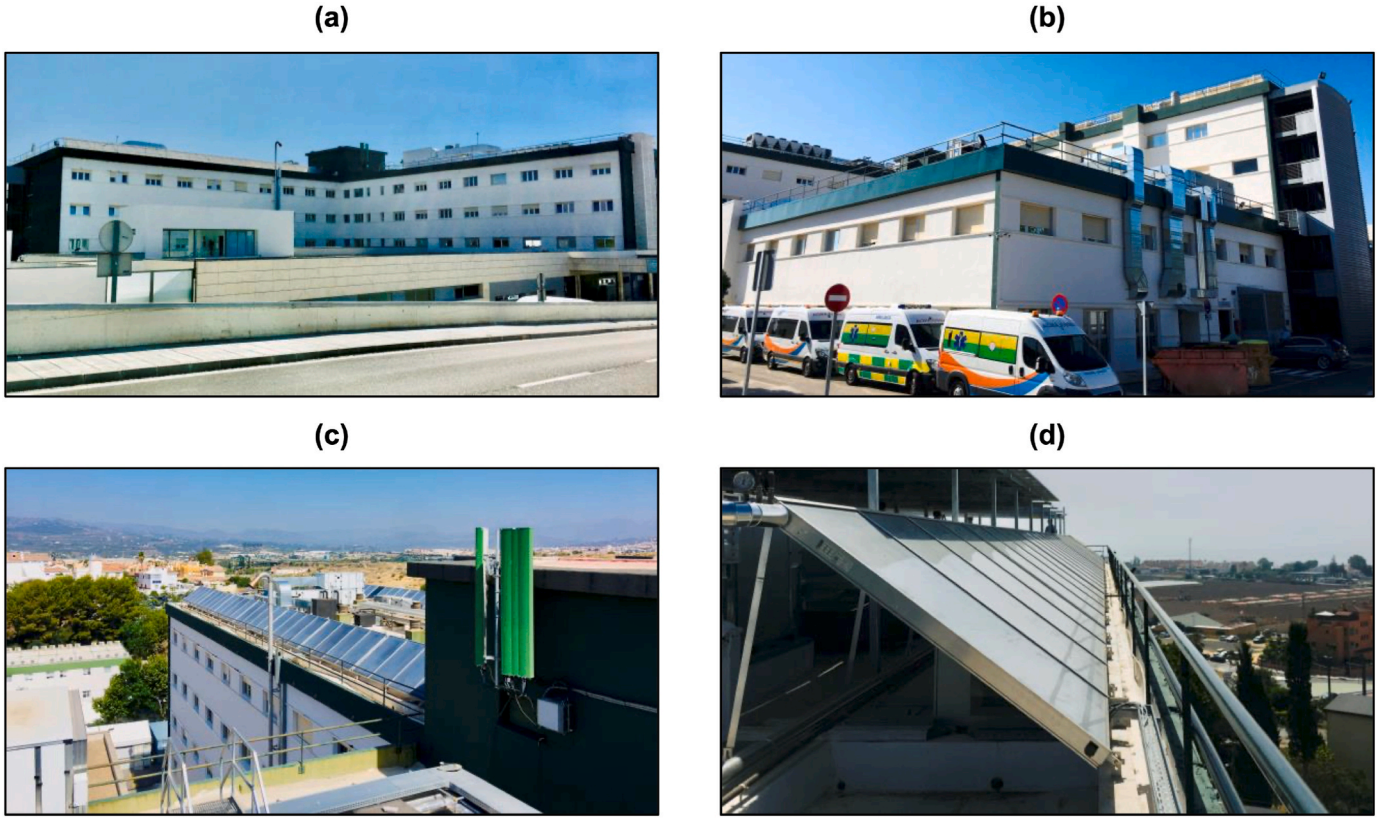

Fig. 1. Case-study hospital. (a, b) External views of the building façade: south (a) and north orientation (b). (c, d) Solar thermal collector branches installed on the roof of the building.

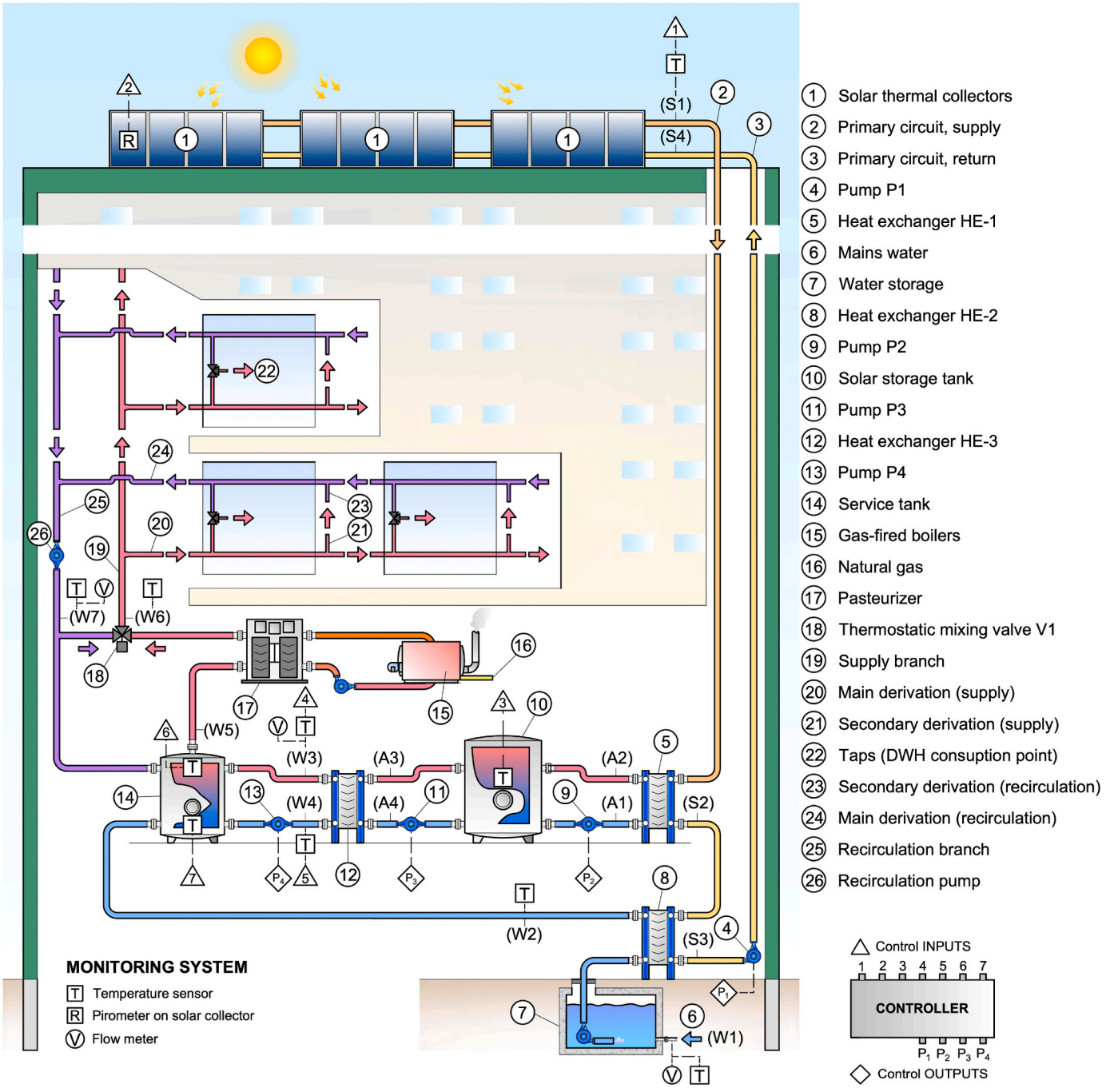

Fig. 2. Schematic layout of the DHW production and distribution system installed in the case-study hospital.

half of the nameplate capacity if that temperature difference falls to 1 °C.

- *Recirculation pump* P_{rec}: always activated.

The three-way thermostatic mixing valve V1 installed downstream of the recirculation pump and upstream of the pasteuriser (Fig. 2), keeps a suitable and constant hot water supply temperature. When the temperature of the service tank is above 60 °C, stream W6 is mixed down to the specified temperature with the cooler recirculated stream W7. These valves are widely used to prevent tap water scald burns [32].

Fig. 2 shows the position of the temperature sensors and flow meters installed in the system for data gathering during the monitoring period between January 2020 and May 2021. In particular, the monitored temperatures and flow rates required to formulate the energy balances written in Section 2.2 are the following: mains water temperature and flow rate (T_{W1}, $\dot{V}_{W1}$, respectively); flow rate through pump P4 ($\dot{V}_{W3}$); temperatures T_{W4} and T_{W3} which corresponds to the streams leaving and entering the heat exchanger HE-3, respectively; temperature of the service tank at its upper level (T_{W5}); temperature of the hot water supplying temperature (T_{W6}); temperature and flow rate of the recirculated stream (T_{W7} and $\dot{V}_{W7}$, respectively).

2.2. Mathematical modelling

The modelling of the system is implemented in TRNSYS 18 [25]. The simulation time-step is set to 5 min. The weather meteorological files required for the simulations were generated using Meteonorm [33]. Table 1 depicts the main size parameters utilised in the simulations. The

Table 1
Main size parameters of the DHW preparation system utilised in the simulations.

Parameter	Value	Comments
Solar collectors' area	180.14 m^2	Flat-plate type 8.578 m^2/collector (net area) and modelled with standard TRNSYS component Type 1 b. Efficiency parameters given as a function of the collector average temperature: intercept efficiency: 0.795; efficiency slope: 3.375 W/(m^2·K); and efficiency curvature: 0.015 W/(m^2·K^2). Tested flow rate: 40 L/(h·m^2). Collector slope: 45°. Ground reflectance: 0.2. It is assumed that the dust deposition on collectors reduces their transmissivity by 2%.
Solar storage tank	10,000 L	Heigh: 5.42 m. Modelled with standard component Type 158 and divided into ten isothermal temperature nodes. Thermal loss (through top and perimeter) coefficient: 2.5 W/(m^2·K).
Service tank	5,000 L	Heigh: 2.71 m. The tank is modelled with component TESS TRNSYS Type 534, that allows multiple entering streams, and is divided into five isothermal nodes. Thermal losses coefficient (top and perimeter): 2.5 W/(m^2·K).
Pumps' nameplate flow rate	P1: 5,000 L/h P2: 6,000 L/h P3 and P4: 5,800 L/h	Variable speed pumps. Component Type 110 utilised in the simulations.
Recirculation flow rate	5,200–9,500 L/h	It was set to 5,200 L/h between January and October 2020 and then, since November 2020, set to 9,500 L/h to solve DHW maldistribution issues and reduce waiting times at consumption points (Fig. 3 (a)). As shown in Fig. 3 (b), the temperature drop was reduced from ~ 6 to 8 °C down to ~ 5 °C.

following modelling assumptions are made:

- All heat exchangers are assumed adiabatic, plate-and-frame type and modelled using standard TRNSYS component Type 91 with constant effectiveness of 0.82. While effectiveness varies with flow rate, the good agreement of simulations results concerning measurements, as shown later in Section 3.1, evidences that this phenomenon is not dominant in this energy system and the constant-effectiveness assumption is valid.
- Pumping groups are modelled as a single circulation pump.
- The supply and recirculation pipes are of the same length.
- The total length of the primary circuit (solar) pipes is assumed 50 m with a thermal loss coefficient of 1.85 W/(m^2·K). Supply and recirculation pipes are considered individually.
- The temperature of conditioned zones is assumed 20 °C and 25 °C during the heating season (set between 15th October and 15th May) and cooling season (16th May and 14th October), respectively.
- The boundary temperature for thermal losses calculation in the solar circuit and storage tanks is calculated by assuming a weighting factor of 0.8 between the outdoor ambient temperature and the temperature of conditioned zones.
- Flow maldistribution through the DHW distribution pipes is not considered.
- The whole DHW distribution network is inside the building.

The global energy balance of the system shown in Fig. 2 is written as follows:

$$\dot{Q}_{SOLAR} + \dot{Q}_b - \left(\dot{Q}_{DHW} + \dot{Q}_{L,pipes} + \dot{Q}_{L,tank2} + \Delta U\right) = 0 \quad (1)$$

where ΔU denotes the variation of internal energy (pipes and service tank) and $\dot{Q}_{L,tank2}$ represents the thermal losses in the service tank. Both the thermal losses through the primary circuit and the solar storage circuit are implicitly included in the net solar production ($\dot{Q}_{SOLAR}$) term. The DHW demand ($\dot{Q}_{DHW}$) is calculated from the following expression:

$$\dot{Q}_{DHW} = \dot{m}_{W1} \times Cp \times (T_{W6} - T_{W1}) \quad (2)$$

The monthly average temperature of the mains water (T_{W1}) is given in Fig. A.1 (Appendix A.1). The solar production is calculated from the energy balance in the heat exchangers HE-2 and HE-3:

$$\dot{Q}_{SOLAR} = \dot{Q}_{HE2} + \dot{Q}_{HE3} = \dot{m}_{W1} \times Cp \times (T_{W2} - T_{W1}) + \dot{m}_{W3} \times Cp \times (T_{W3} - T_{W4}) \quad (3)$$

On the other hand, the thermal energy supplied to the DHW stream from the boilers and through the pasteuriser ($\dot{Q}_b$) is calculated as follows:

$$\dot{Q}_b = \begin{cases} (\dot{m}_{W1} + \dot{m}_{W7}) \times Cp \times (60°C - T_{W5}), & T_{W5} < 60°C \\ 0, & Otherwise \end{cases} \quad (4)$$

The natural gas consumption rate as fuel in the boilers ($\dot{V}_G$, in m^3/s) is calculated from the following equation:

$$\dot{V}_G = \dot{Q}_b / (LHV \times \eta_b) \quad (5)$$

where the lower heating value (*LHV*) of natural gas and the efficiency of the boiler (η_b) are assumed 10.08 kWh/m^3 and 90%, respectively.

On the other hand, the emission factor (*EF*) of natural gas is assumed 200 kg-$CO_{2,eq}$/MWh and the GHG emissions (*GHGe*) generated from its combustion are calculated as follows:

$$GHGe = \dot{V}_G \times LHV \times EF \quad (6)$$

The total thermal losses of the recirculated flow rate through the DHW distribution network (both supply and recirculation pipes) are calculated as follows:

$$\dot{Q}_{L,pipes} = \dot{m}_{W7} \times Cp \times (T_{W6} - T_{W7}) \quad (7)$$

Finally, the solar contribution (so-called *solar* fraction, *SF*) is defined as follows:

$$SF = \dot{Q}_{SOLAR} \Big/ (\dot{Q}_{SOLAR} + \dot{Q}_b) = \dot{Q}_{SOLAR} \Big/ \left(\dot{Q}_{DHW} + \sum \dot{Q}_L\right) \quad (8)$$

where the summation term includes both the thermal losses through the hot water pipes and the service tank.

The energy flows and the solar fraction defined above can be calculated from the data gathered from the temperature sensors and flow meters installed in the system (see Fig. 2). The uncertainty for the measured temperatures in °C is $\pm(0.3 + 0.005 \cdot |T|)$ which corresponds to tolerance class B temperature sensors [34]. As for the flow rates, the uncertainty is ±5% of the measured value. In both cases, the coverage factor is 2. The uncertainty propagation method described in the NIST Technical Note 1297 [35] is applied to estimate the error bounds of the quantities calculated from the monitored variables, which are later used in Section 3.1 to assess the validity of the modelling developed in TRNSYS.

2.2.1. Modelling of hot water demand and recirculation flow rates

The hourly DHW demand in hospitals can be estimated in different ways. In the case of new-built projects, an option to estimate the demand is to use standard profiles and assume average consumptions (e.g., as a function of the number of beds or hospital building's surface [36]). However, the DWH demand in buildings varies across location and depending on the services provided, among other factors [37]. Thus, standard profiles typically deviate from reality [38]. DHW demand profile generators tools could be an interesting alternative when

consumption data are lacking [39]. In the case of existing buildings, the demand could be estimated using previous measurements.

In this paper, the consumption data gathered during a year and a half are used to develop a straightforward method that allows estimating the hourly DHW in the case-study hospital building. The cumulative monthly demand was also analysed to determine the seasonal behaviour.

The hourly DHW demand (in L/h) is calculated from the following mathematical expression:

$$D_{DHW} = \alpha \times \beta \times \varphi \tag{9}$$

where α represents the reference *peak* demand rate and is set to 1,600 L/h. The dimensionless parameter β shown in Fig. 4 (a) represents the ratio between the hot water demand for each hour of the day and the peak hourly demand registered throughout the week. The assignation of the β-values that shape the hourly demand profile is consistent with the patterns of demand observed for different types of days (weekdays, Saturdays and Sundays) during the period in which the system was monitored (i.e., between January 2020 and May 2021). Since it was observed that the shape of the hourly demand profile was almost constant regardless of the month of the year, a single dimensionless hourly profile can be used.

The profile is characterised by a high degree of irregularity, as shown in Fig. 4 (a). This phenomenon agrees with the observations of Bujak [40]. The lowest demand is observed between 23:00 to 6:00, while the highest consumption is observed between 8:00 and 21:00. The demand is lower on weekends since few activities are scheduled in the hospital.

The dimensionless parameter φ in Fig. 4 (b) is a monthly scaling factor that introduces the seasonal demand variation. Note that a value of $\varphi = 1$ is assigned to the month that, according to the measurements, registered the highest DHW demand during the monitoring period (i.e., November 2020: 12,646 L/day). The demand generally increases in the heating season.

To assess the validity of this simplified method developed to forecast the hot water demand, the deviation between the monitored demand and the simulation results are analysed in Section 3.1.

2.2.2. Modelling of the hot water distribution network

The DHW distribution network of large buildings such as hospitals is plenty of particularities, and there are numerous pipe section sizes (length and diameters). Nonetheless, the model developed in this work has been simplified by grouping the pipes (modelled with the standard TRNSYS component Type 31) into the following categories (see Fig. 2):

1) *Main branches.* Equivalent inner diameters: 44.7 mm (supply) and 25.8 mm (recirculation). Total length: 252 m.
2) *Main derivations.* Equivalent inner diameters: 62.0 mm (supply) and 30.5 mm (recirculation). Total length: 779 m.
3) *Secondary derivations.* Equivalent inner diameters: 27.1 mm (supply) and 25.0 mm (recirculation). Total length: 443 m.

These equivalent diameters rely upon the average found for each pipe category. Considering the pipe lengths estimated from the installation drawings, the total heat transfer area of the DHW distribution network is estimated at 177.5 m^2, while the considered in the design stage was 30.5 m^2. The equivalent overall heat transfer coefficient (UA_{eq}) of the DHW distribution network is determined from steady-state periods (i.e., without DHW demand) using the following expression:

$$\dot{Q}_{L,pipes} = UA_{eq} \times \frac{(T_{W6} - T_{amb}) - (T_{W7} - T_{amb})}{ln[(T_{W6} - T_{amb})/(T_{W7} - T_{amb})]} \tag{10}$$

The temperature of the ambient surrounding the pipes (T_{amb}) is assumed equal to the temperature of conditioned zones since the hot water pipes run through interior spaces such as wall cavities or suspended ceilings. Fig. 5 illustrates the equivalent *UA* estimated for the DHW distribution network: ~1.1–1.7 kW/K. Therefore, the *U*-value ranges between ~6.2 and 9.6 W/(m^2·K), which is well above the assumed in the design, i.e., 2.38 and 2.54 W/(m^2·K) for the supply and recirculation pipes, respectively. Regarding simulations, it is set to the average value found, i.e., 8 W/(m^2·K).

2.2.3. Model validation indicators

The modelling is calibrated on a monthly basis. The indicators used to determine the accuracy of the model outputs concerning the measurements are the normalized mean bias error (*NMBE*) and coefficient of variation of the root-mean square error (*CV(RMSE)*). Their mathematical definitions are:

$$NMBE = \frac{1}{\overline{m}} \cdot \frac{\sum_{i=1}^{N} (y_{exp,i} - y_{sim,i})}{(N-p)} \times 100\% \tag{11}$$

$$CV(RMSE) = \frac{1}{\overline{m}} \sqrt{\frac{\sum_{i=1}^{N} (y_{exp,i} - y_{sim,i})^2}{N-p}} \times 100\% \tag{12}$$

where y_{exp} and y_{sim} are the monthly quantities calculated from the measurements and the monthly simulation results, respectively, N is the number of months during which the system was monitored. The term $\overline{m}$ is the mean of the monthly quantities calculated from the measure-

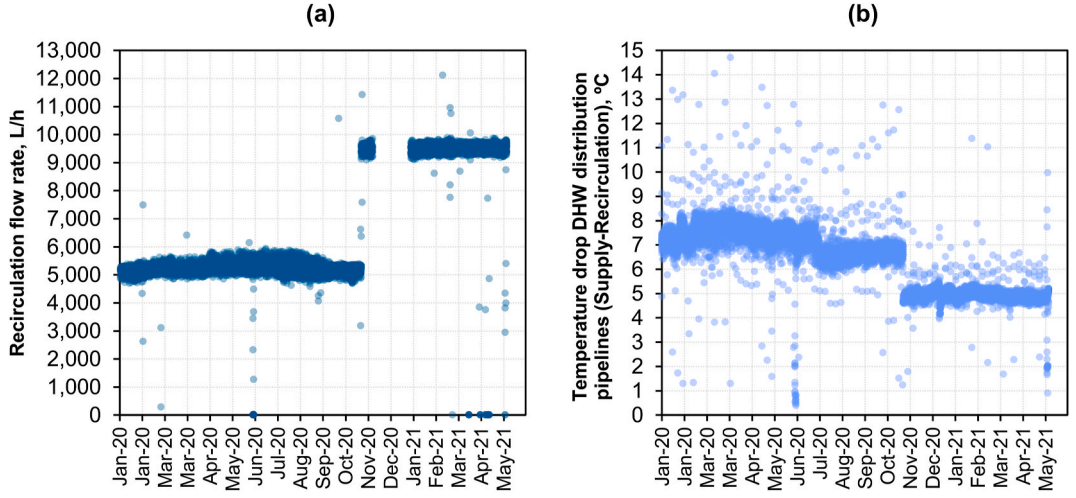

Fig. 3. Monitored variables from January 2020 to May 2021. (a) Recirculation flow rate (data gap between December 2020 and January 2021). (b) Temperature drop (supply-recirculation) through the DHW distribution network.

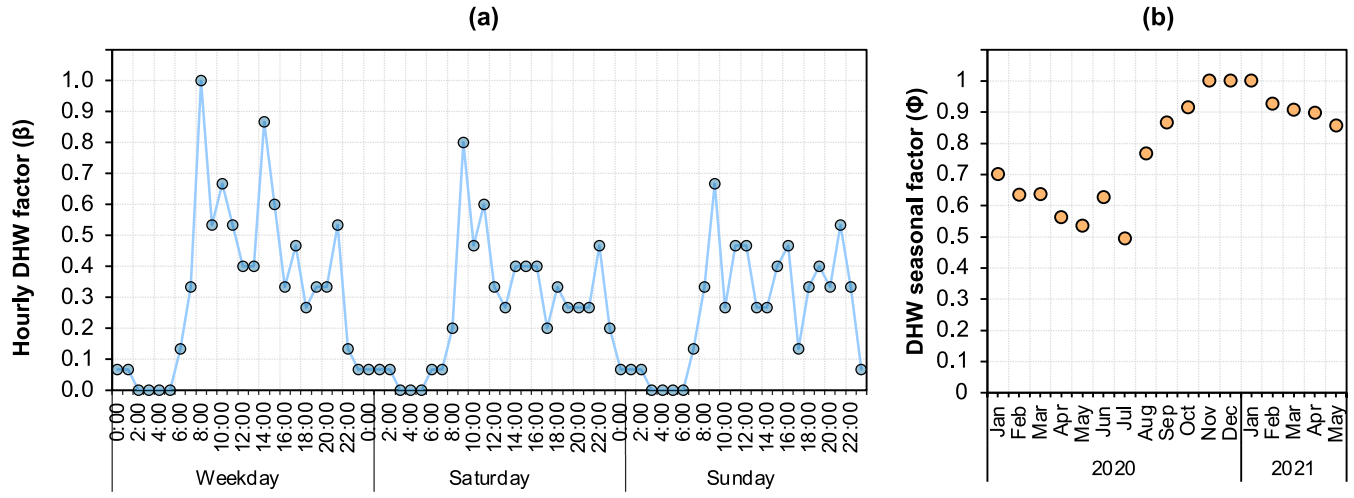

Fig. 4. Parameters for the modelling of the DHW demand utilised in Eq. (9). (a) Generic hourly profile for weekdays and weekends. (b) Seasonal factor. Data gap between December 2020 and January 2021; thereby, the seasonal factor for November is utilised for these months in the simulations.

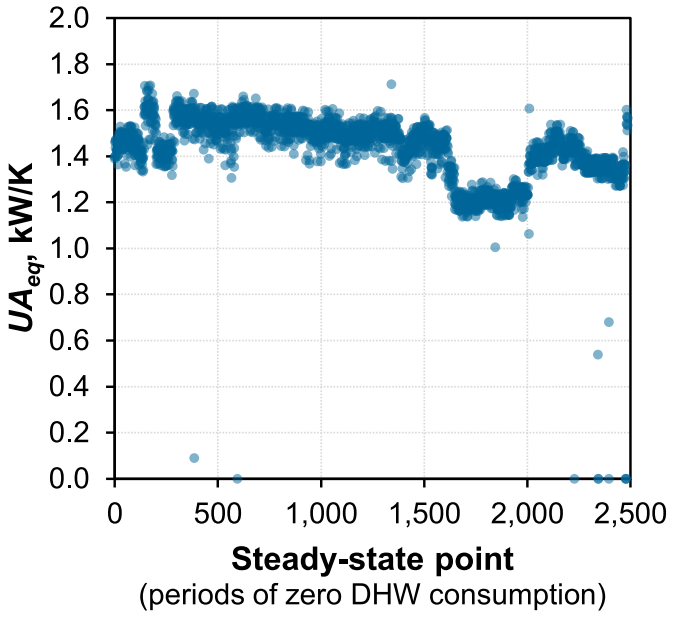

Fig. 5. Equivalent overall heat transfer coefficient (UA_{eq}, Eq. (10)) of the DHW distribution network calculated in steady state points (i.e., periods without DHW consumption) and obtained from the long-term monitoring of the installation.

ments, with p set to one. The acceptable criteria for monthly calibration data is ±5% and 15% for the *NMBE* and *CV(RMSE)*, respectively [41].

2.3. Economic analysis

The economic feasibility of the energy retrofit measures is evaluated through a new indicator so-called *levelised cost of hot water* (LCoHW), in €/kWh. This parameter indicates the present value of the total cost of producing a unit of hot water (in terms of thermal energy) over the whole system's lifetime. Its mathematical definition is as follows:

$$LCoHW = \frac{TCI + \sum_{k=1}^{n}\left[AE_k \times (1+r)^{-k}\right]}{\sum_{k=1}^{n}\left[Q_{DHW,k} \times (1+r)^{-k}\right]} \tag{13}$$

The term $Q_{DHW,k}$ is the DHW demand (in kWh) throughout year k. The parameters n and r represent the installation lifetime (15 years) and the annual discount rate (0.10 [42]), respectively.

The total capital investment (*TCI*) required for the energy retrofit is divided into the Fixed Capital Investment (*FCI*), and the working capital and the start-up cost, assumed as 10% and 5% of the *FCI*, respectively. The *FCI* splits into the Purchased Equipment Cost (*PEC*, assumed equal to the free on-board cost – FOB – destination, freight prepaid) of the new equipment required by the energy refurbishment, which is estimated from the cost functions given in Table A.1 (Appendix A.2), and other fixed costs (*OFCs*) estimated as a fraction of the total *PEC* of these newly installed components [43]: installation (20%), piping (10%), instrumentation and control (6%) and electric equipment and material (10%).

On the other hand, the annual expenses (*AE*) of the installation in year k are due to due to electricity, gas, and water bills, the carbon taxes, and other annual expenditures (*OAE*), for example, maintenance, insurance and taxes, and annual overhead costs, which are estimated as 6%, 1% and 1%, respectively, of the fixed capital value (i.e., purchase cost and other fixed costs) of both the already existing and the new components required by the energy refurbishment:

$$AE_k = \left\{ \int_{i=0}^{i=8760\ h} \left[W_{el,net}(i) \times C_e(i)\right] + V_G \times HHV \times C_G + V_{DHW} \times C_w + GHGe \times C_{CO_2} + OAE \right\}_k \tag{14}$$

As explained in Appendix A.2, the electricity bill is calculated from the net annual electricity consumption ($W_{el,net}$) and the electricity tariff (C_e, €/kWh) which depends on the hour of the day and the month (see Table A.2.). Note that the electricity consumed in the hospital is assumed to be supplied by a company that sells electricity generated only from renewable sources (i.e., null GHG emission factor). The gas bill is calculated from the gas consumed throughout the year (V_G, m^3), the higher heating value of natural gas (*HHV*, assumed 11.70 kWh/m^3), the gas tariff (C_G, set at 50 €/MWh) and the carbon taxes imposed (C_{CO_2}, €/t-$CO_{2,eq}$). The water bill is calculated from the volume of DHW consumed and the water tariff (C_w, assumed 1.20 €/m^3). No subsidies to promote the installation of renewable energy technologies are considered in the economic study.

Regarding carbon taxes (C_{CO_2}), the following climate policy scenarios are considered:

1) *Business-as-usual* (BAU) scenario. Least ambitious scenario since no carbon taxes are imposed due to in-situ GHG emissions in the hospital.

2) *Sustainable development scenario* (SDS). Carbon price set to 120 €/t-$CO_{2,eq}$.
3) *Zero emissions scenario* (ZES). Carbon price set to 600 €/t-$CO_{2,eq}$ [44]. This case includes stronger global action to reduce emissions and more rapid advances in low-carbon technologies.

The conclusions derived from the economic analysis presented in section 3.2 are constrained by the hypothesis and the value set to the parameters involved in the calculation of the LCoHW. Therefore, they should be modified according to the specific context of each particular energy retrofit project.

3. Results and discussion

3.1. Energy audit and model calibration

Fig. 6 shows the monthly results obtained from the monitoring of the installation from January 2020 to May 2021, and the shaded areas represent the uncertainty bounds with a coverage level of 95%. These results are benchmarked against those reported by the model, and the assumed at the design stage. Note that monitoring data are missing between December 2020 and January 2021. Table 2 provides a summary of the annual performance parameters. The following observations can be made:

- As shown in Fig. 6 (a), there are remarkable differences between the DHW consumption considered in the design values and the monitored from January to August 2020 mainly because the Covid-19 pandemic altered the typical activity in the hospital (and also in other types of buildings [45]). Since that date, design values match the actual demand. Regarding simulations, the simplified model described in Section 2.2.1 calculates the monthly DHW demand accurately (*NMBE* = 3.9%; *CV(RMSE)* = 4.7%) and with very low computational cost.
- Fig. 6 (b) shows that solar production increases during periods with higher radiation levels (i.e., May–September). The deviation of the

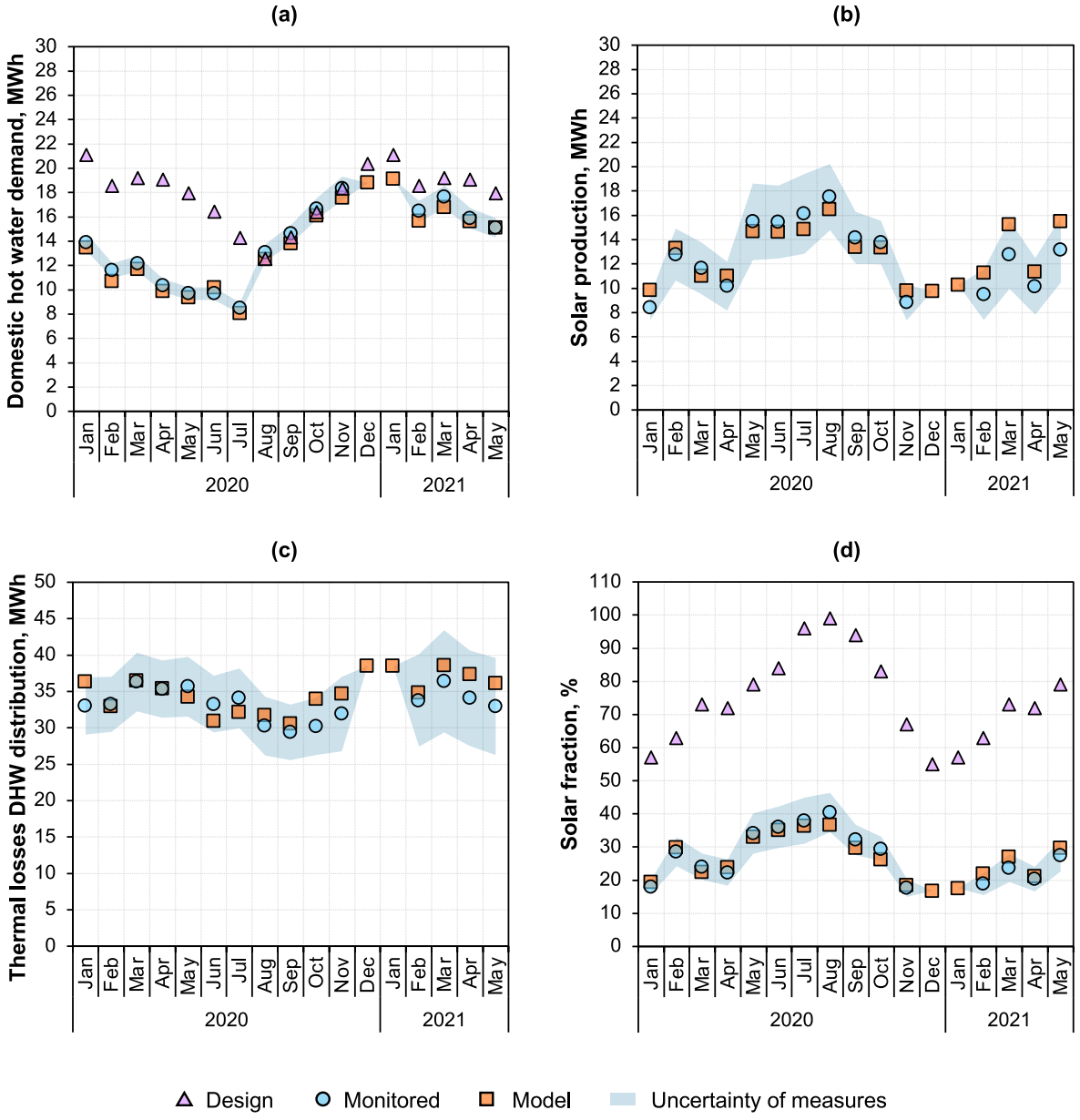

Fig. 6. Monthly performance parameters between January 2020 and May 2021 corresponding to the design, monitoring of the system, and simulation results. (a) DHW demand, (b) Solar production, (c) Thermal losses through the DHW distribution pipes, and (d) Solar fraction.

Table 2
Annual project data versus monitored and simulated.

Performance parameters	Case				
	Design	Monitored system		Simulations	
		Jan.–Nov. 2020	Feb.–May 2021	2020 (Jan.–Nov.)	Jan–May 2021 (Feb.–May)
DHW demand, MWh/y	208.54	138.54	65.04	152.00 (133.21)	82.22 (63.12)
Solar production, MWh/y	181.83[a], 169.4[b]	144.34[b]	45.56[b]	152.12 (142.37)[b]	63.68 (53.39)[b]
Thermal losses through distribution pipes) MWh/y	16.79	362.56	137.13	407.81 (369.31)	185.38 (146.90)
Thermal losses (service tank), MWh/y	–	10.54	2.58	11.6 (10.46)	5.47 (4.30)
Thermal energy supplied from boilers, MWh/y	56.41	367.30	159.18	418.59 (369.94)	209.24 (160.66)
Estimated natural gas consumption (Eq. (5)), m^3	6,218	40,487	17,546	46,141 (40,778)	23,064 (17,709)
GHG emissions (Eq. (6)), t-$CO_{2,eq}$	12.5	81.6	35.4	93.0 (82.2)	46.5 (35.7)
Solar fraction (Eq. (8)), %	75.2	28.2	22.3	26.6 (27.8)	23.3 (24.9)

[a] Thermal energy supplied from the solar collectors to the primary fluid circuit.
[b] Thermal energy exchange in the heat exchangers HE-2 and HE-3 (Fig. 2). Including thermal losses both in the primary fluid circuit and solar storage circuit.

modelling concerning the actual solar production is within the allowable calibration limits (*NMBE* = −3.4%; *CV(RMSE)* = 10.9%).

- As shown in Fig. 6 (c), the model predicts the thermal losses through the DHW distribution pipes with acceptable accuracy (*NMBE* = −3.6%; *CV(RMSE)* = 7.0%). However, thermal losses given in Table 2 are far above the design expectations; in fact, they are even higher than the DHW demand. The reasons are (1) poor insulation of DHW pipes, leading to high *U*-values as discussed in Section 2.2.2, and (2) the existing DHW distribution network is lengthier than assumed in the design. The thermography shown in Fig. 7 verifies the thermal insulation issues. In a visual inspection, the authors observed the multiple defects in the insulation material, for example, those shown in Fig. 7 (a) and Fig. 7 (b); even some bare pipes are observed (Fig. 7 (c)). There are also valves and accessories that are badly insulated, as shown in Fig. 7 (d). Other authors [31] also discussed the large share of thermal losses concerning the total energy consumption of hot water preparation systems in other types of buildings.
- Fig. 6 (d) remarks that the solar fraction is well below design expectations mainly because of the above-mentioned massive thermal losses. Though the system was engineered to handle more than 90% of the DHW demand with the solar production between July and September, the actual solar contribution hardly reaches 30–40% in this period. As shown in Table 2, the projected annual solar fraction was 75%, while that of the current system is barely 27%. The model also reproduces accurately the solar fraction calculated from the motoring data (*NMBE* = 0.1%; *CV(RMSE)* = 8.6%). Hence, the modelling accomplishes the monthly calibration criteria for all the variables compared and, in every month, the simulation results are within the uncertainty bounds of the quantities calculated from the monitored variables.
- As shown in Table 2, the DHW system was engineered for consume around 6,000 m^3 of natural gas (i.e., GHG emissions of 12 t-$CO_{2,eq}$). However, because of the massive thermal losses, the gas consumption and GHG emissions of the current installation are above 40,000 m^3 and 90 t-$CO_{2,eq}$, respectively.

3.2. Evaluation of energy retrofit measures

Based on the audit results, the following energy retrofit measures are considered to achieve a target solar fraction of 60% and reduce the carbon footprint of the DHW system:

1) Improvement of the **thermal insulation** of DHW distribution pipes. The *U*-values considered range between values close to the assumed in the design and that of the current system (i.e., ~2–8 W/(m^2·K), respectively).
2) Extension of the existing **solar field** by adding up to six extra solar collectors per branch.

Furthermore, installing a high-temperature water-to-water heat pump could be an attractive energy efficiency measure. As shown in Fig. 8, it will be installed between the recirculation manifold and the service tank to cope with the thermal losses through the DHW distribution pipes and curb the gas consumption and GHG emissions. Besides, the chilled water produced in the evaporator at 7 °C could be used as a by-product for air-conditioning applications since there is always refrigeration demand in the hospital. The heat pump could perform more efficiently if installed downstream of the heat exchanger HE-2 because of lower condensing temperatures. However, the utilization rate would be lower since it would activate only in periods of DHW demand. The modelling is described in Appendix A.2.

To evaluate the energy retrofit measures, the recirculation flow rate is set to 9,500 L/h, and the weather file and DHW demand profile used in the simulations corresponds to the data gathered during the year 2020. Table 3 depicts the simulation results for the following cases: current system without any enhancement (Case A) and with the installation of a 61-kW heat pump (A w/HP) but without improvement of the thermal insulation of hot water pipes nor the addition of extra collectors to the solar field; Cost optimised energy retrofit solution to reach the 60% solar contribution without and with the installation of a 26-kW heat pump (Case B w/HP and B w/o HP, respectively).

Fig. 9 depicts the solar fraction and LCoHW calculated for different climate policy scenarios. Table 4 shows the breakdown of capital costs and annual expenses. Finally, Fig. 10 shows the total capital investment required and the gas or electricity consumptions.

The following observations are made:

- As shown in Table 3, the gas consumption and on-site GHG emissions are significantly reduced by installing a heat pump. Without implementing any energy retrofit measure, installing a heat pump is a promising energy efficiency solution to boost the system's economic performance. Indeed, the LCoHW of the current installation may be reduced by 27% if no carbon taxes were imposed (i.e., from 37.1 down to 28.6 cent-€/kWh), and even to 61% in an ambitious climate policy scenario (i.e., from 75.2 down to 29.0 cent-€/kWh). Nevertheless, the solar fraction remains scanty because of the vast thermal losses, so the thermal insulation upgrade and/or the addition of solar collectors are still required to achieve the target solar fraction. However, this will lead to higher capital investment (see Table 4) and LCoHW, as displayed in Fig. 9 (a).
- To limit the thermal losses and reach the target solar fraction, the *U*-value of the DHW distribution network should be reduced below 3.5 W/(m^2·K). The optimal techno-economic solution lies in a trade-off between the quality of the upgraded pipes insulation and the number of extra collectors added. For energy retrofit packages without heat pump (Fig. 10 (a)), the capital cost increases with the insulation quality. In contrast, for retrofit solutions with installation of a heat pump, the investment could decrease as the insulation level

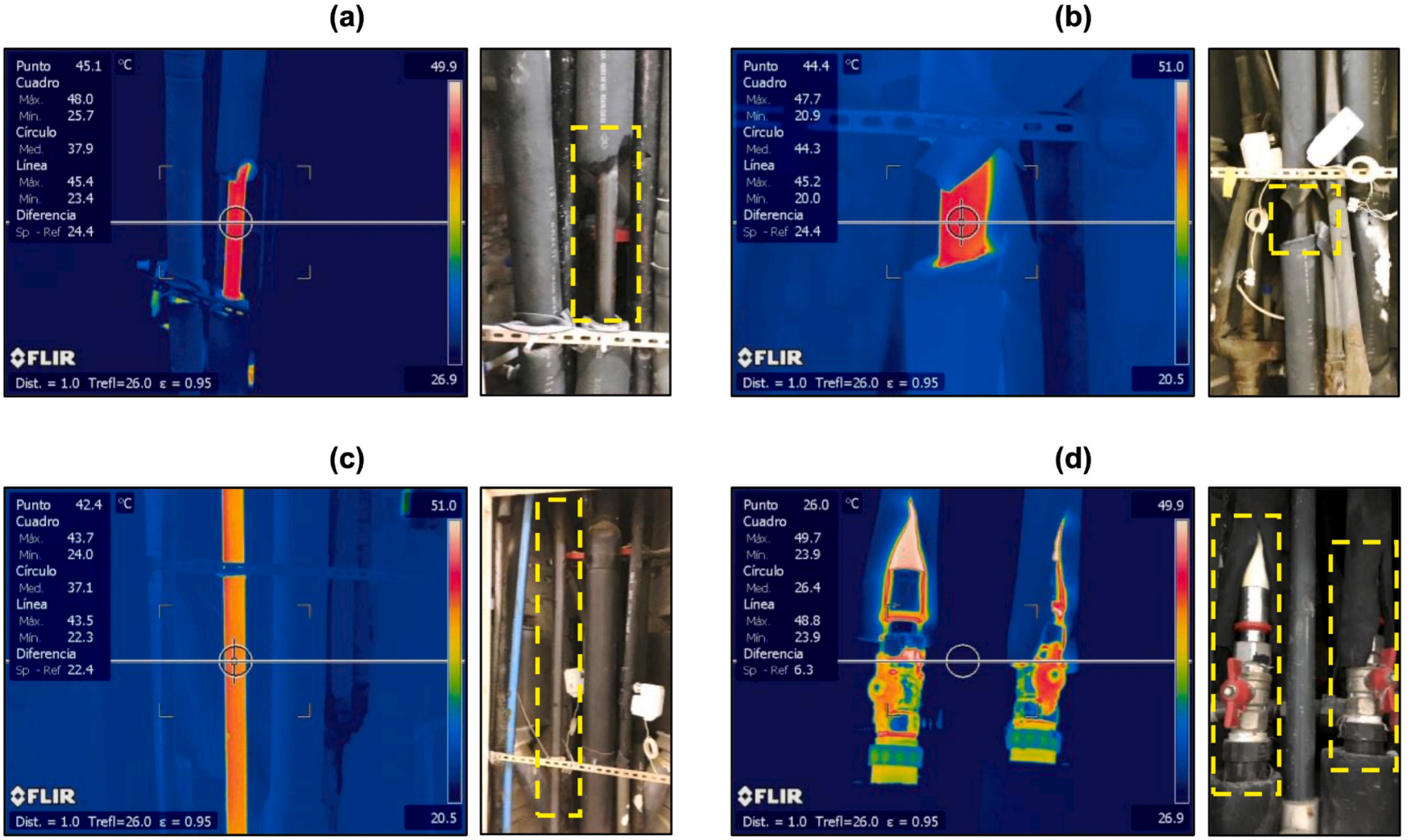

Fig. 7. Thermography of some sections and pipes of the DHW distribution network obtained in a walkthrough inspection. (a, b) Defects in the thermal insulation some points. (c) Pipe without thermal insulation. (d) Valves poorly insulated.

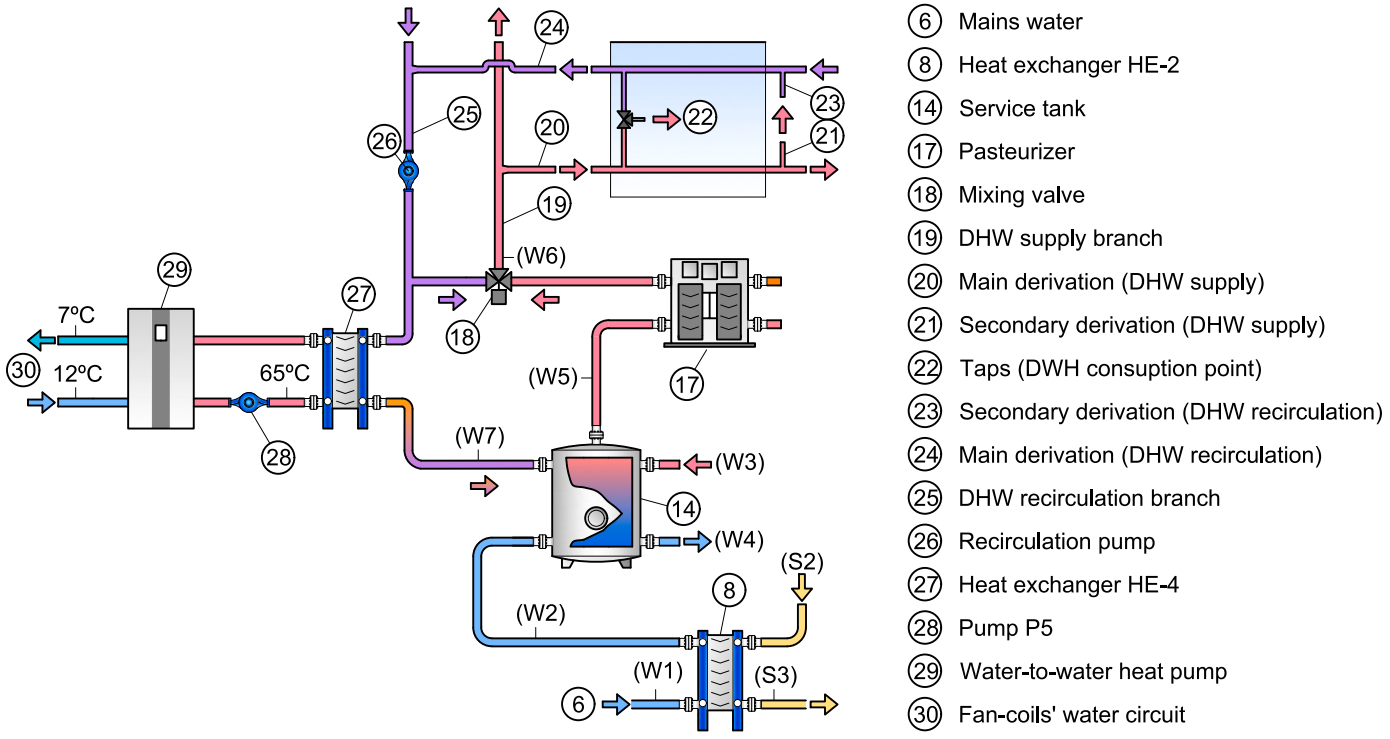

Fig. 8. Schematic layout of the system with an installed high-temperature water-to-water heat pump. The numbering of system components is consistent with Fig. 2.

Table 3
Annual simulation results for the actual installation and for the different energy retrofit packages considered.

Case	U-value DHW pipes, W/(m^2·K)	No. solar col.	Thermal losses, MWh/y	SF, %	Energy consumption				Utility bill, thousand-€/year					LCoHW, cent-€/kWh		
					Gas, m^3/y (GHGe, t-$CO_{2,eq}$/year)	Electricity, MWh/y			Gas (including carbon taxes)			Water	Electricity (A/C[a])			
						Heat pump	Pumps	A/C[a]	BAU	SDS	ZES			BAU	SDS	ZES
A	8.00	21	443.4	24.9	49,716 (100)	0	13.7	0	29.1	39.1	89.2	4.0	1.4 (0)	37.1	43.5	75.2
A w/ HP	8.00	21	444.7	22.5	548 (1.10)	160.4	15.5	−101.2	0.3	0.4	1.0	4.0	7.7 (−10.3)	28.6	28.6	29.0
B w/o HP (BAU and SDS)	2.50	30	145.1	60.3	13,717 (27.7)	0	14.4	0	8.0	10.8	–	4.0	1.5 (0)	31.1	32.9	–
B w/o HP (ZES)	2.25	30	130.9	62.6	12,354 (24.9)	0	14.4	0	–	–	22.2	4.0	1.5 (0)	–	–	40.8
B w/HP	2.25	33	131.5	62.3	2,989 (6.03)	32.8	15.1	−18.1	1.7	2.4	5.4	4.0	3.0 (−1.8)	33.8	34.2	36.1

Notes: Case A: current system. Case A w/HP: Current system with installation of a 61-kW heat pump (A w/HP). Case B: Cost optimised energy retrofit solution to reach the 60% solar contribution without heat pump (Case B w/o HP) and with installation of a 26-kW heat pump (Case B w/HP). Scenarios for application of carbon taxes: Business-*as*-usual (BAU, 0 €/t-$CO_{2,eq}$); Sustainable development Scenario (SDS, 100 €/t-$CO_{2,eq}$); Net-zero emissions scenario (NZE, 600 €/t-$CO_{2,eq}$).

[a] Saving due to the chilled water produced as by-product in the heat pump and used for air-conditioning applications.

improves up to a medium quality (i.e., < ~4 W/(m^2·K), see Fig. 10 (b)) since the heat pump installed would smaller. However, the investment soars for thicker insulations (i.e., < ~2 W/(m^2·K)) because the purchase cost increases as dramatically (see Fig. A.2., Appendix A.2). In either case, the addition of solar collectors also significantly impacts the investment.

- The cost-optimised energy retrofit solution is generally found for *U*-values of the DHW distribution circuit within the range 2.25–2.50 W/(m^2·K) and the addition of 3–4 solar collectors per branch. Hence, thermal losses would be reduced by roughly 70% and the current net caption area would be enlarged from 180 to 257–283 m^2 (i.e., by 43–57%). However, the optimal solution depends ultimately on the ongoing climate goals. For instance, if GHG emissions were unpunished (Fig. 9 (b)), the most cost-effective retrofit solution consists of upgrading the DHW pipes insulation up to 2.50 W/(m^2·K) and installing nine extra collectors, without a heat pump. Then, the current system's gas consumption in boilers would be reduced by 72%, and the LCoHW may drop from 37.1 to 31.1 cent-€/kWh.
- Regarding the sustainable development scenario (Fig. 9 (a) and (c)), the LCoHW of the refurbished system is estimated at 34.2 and 32.9 cent-€/kWh for the case with and without the installation of a heat pump, respectively. Thus, the heavy capital investment associated

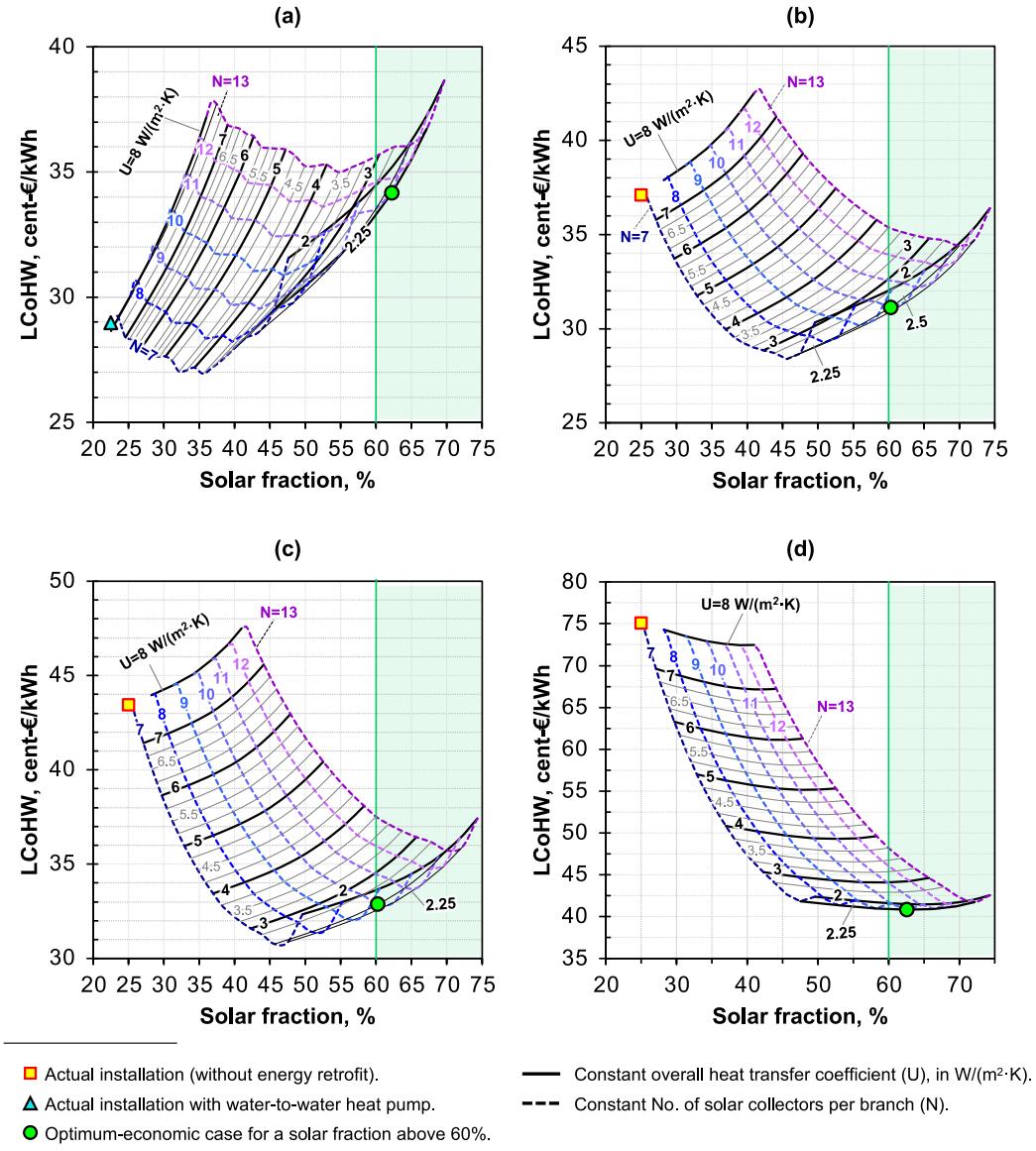

Fig. 9. Annual solar fractions and levelised costs of hot water production for different *U*-values of DHW pipes and solar collectors. (a) Energy retrofitting with installation of a water-to-water heat pump in the Sustainable Development Scenario. Energy retrofitting solutions without heat pump: (b) Business-*as*-usual, (c) Sustainable development scenario, and (d) Net-zero emissions scenario.

with a heat pump (given in Table 4) yet outweighs its economic benefits because of lower gas consumption and GHG emissions. Nevertheless, in the context of ambitious climate policies, the carbon taxes avoided throughout the system life span are of great economic value (Table 3). Indeed, in the net-zero emissions scenario, the optimal retrofit solution to achieve the target solar fraction consists of installing a heat pump, upgrading the *U*-value of DHW pipes up to 2.25 W/(m^2·K), and adding twelve extra solar collectors. The LCoHW is estimated to be 36.1 cent-€/kWh, which is 20% lower than a refurbished system without a heat pump (i.e., 40.8 cent-€/kWh).

4. Conclusions

This paper focused on the energy audit and evaluation of energy retrofit measures to boost the solar fraction of the domestic hot water system of an existing medium-size hospital building. The following conclusions can be drawn:

1. The vast ongoing thermal loss throughout the hot water distribution network explains the poor solar fraction of the system (<30%) concerning the system design (75%). In a nutshell, the deficient thermal insulation (because of both a poor installation and deterioration with time) and the underestimation of the heat transfer area of the hot water distribution network explain why heat losses are far above the design expectations. Although it may sound trivial, this is an endemic technical issue observed in hot water-intensive buildings such as hospitals.
2. The cost-optimised energy retrofit solution to enhance the solar fraction up to 60% consists of reducing thermal losses by 70% and expanding the current solar caption area by 43–57%, depending on the climate policies imposed. The refurbished system could reduce the levelised cost of hot water production by 16% (i.e., from 37.1 to 31.1 cent-€ kWh) compared to the current system if GHG emissions were free from carbon taxes. In a context of more ambitious climate policies, installing a heat pump is an attractive energy efficiency measure to greatly reduce gas consumption and emissions, thereby enhancing the economic competitiveness of the system.
3. The particular features and assumptions involved in this study constraints the extrapolation of the energy retrofit recommendations to other case-study buildings. Nonetheless, the indicators and charts

Table 4
Breakdown of cost (in thousand-€) for the current installation and for the energy refurbishment cases with and without heat pump and for the different climate policies scenarios considered.

Costs	Baseline-case without energy retrofit	Actual system with installation of a heat pump	Energy retrofit option with solar fraction >60% and minimum LCoHW			
			Without heat pump			With heat pump
			BAU	SDS	ZES	
• **Total Capital Investment (TCI)**	–	**45.6**	**58.5**	**58.5**	**65.0**	**104.8**
1. Fixed Capital Investment (FCI):	–	39.7	50.9	50.9	56.5	91.2
1.1. Purchase equipment cost (PEC) of new components:	–	27.2	34.8	34.8	38.7	62.4
1.1.1. Insulation material DHW distribution pipes	–	0.0	13.1	13.1	16.9	16.9 (26)
1.1.2. Solar thermal collectors	–	0.0	21.8	21.8	21.8	29.0 (6)
1.1.5. Heat pump (rated heating capacity, kW)	–	18.6 (61)	–	–	–	11.4 (1.6)
1.1.6. Pump P5 (power, W)	–	0.35 (21)	–	–	–	0.13
1.1.7. Heat exchanger HE-4 (area, m^2)	–	8.3 (3.6)	–	–	–	4.9
1.2. Other fixed costs (OFCs)	–	12.5	16.0	16.0	17.8	28.7
2. Working capital	–	4.0	5.1	5.1	5.7	9.1
3. Start-up cost	–	2.0	2.5	2.5	2.8	4.6
• **Fixed capital value of the whole installation**	**273.7**	**313.3**	**324.5**	**324.5**	**330.2**	**364.8**
1.1. Total Purchase value of equipment[a]	187.4	214.6	222.3	222.3	226.2	249.9
1.2.Other fixed costs (OFCs)	86.2	98.7	102.2	102.2	104.0	114.9
• **Other annual expenses of the installation (*OAE*)**[b]	**21.9**	**25.1**	**26.0**	**26.0**	**26.4**	**29.2**
1. Operation and maintenance	16.4	18.8	19.5	19.5	19.8	21.9
2. Insurance and taxes	2.7	3.1	3.2	3.2	3.3	3.6
3. Overheads	2.7	3.1	3.2	3.2	3.3	3.6

[a] Purchased cost value estimated (in thousand-€) of equipment currently installed: Heat exchangers H3-1 … 3: 32.7; Gas boiler (440 kW): 82.3; Pasteuriser (390 kW): 35.2; Pumps P1 … 4 and P_{rec}: 1.8; Tank 1 (solar, 10 m^3): 20.8; Tank 2 (service, 5 m^3):14.1; Insulation primary circuit: 0.58.
[b] Expenses based on the fixed capital value of all the system components (newly installed and already existing equipment).

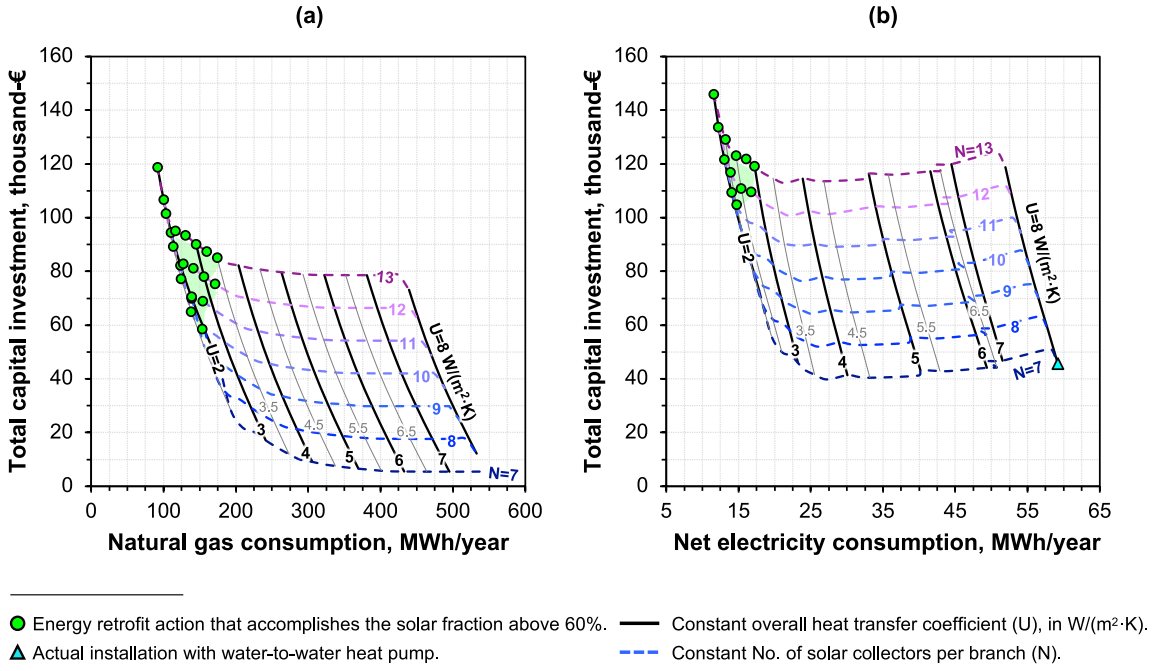

Fig. 10. Total capital investment required for different combinations of solar thermal collectors installed and *U*-values of DHW pipes. (a) Without heat pump. (b) With installation of a water-to-water heat pump.

developed in this paper provide engineers with valuable tools to streamline the decision-making process concerning the selection of cost-optimised energy retrofit measures for domestic hot water systems in hospitals and other hot water-intensive buildings. Furthermore, the methodology presented is flexible and could consider numerous constraints. Examples are limited project budget and resources, specific solar contribution targets, limited roof surface to extend the solar field, or structural constraints that block the improvement of thermal insulations.

Future research can focus on developing reliable design methodologies for solar DHW systems in new-built hospital buildings. An integrated analysis approach will be implemented to identify those design parameters with major influence on the energy performance. The aim

will be to factor the uncertainties into the design process to ensure that the desired performance is met despite deviations in the operating conditions or quality of maintenance. Hence, subsequent energy audits and energy refurbishment actions would be avoided.

Declaration of competing interest

The authors declare that they have no known competing financial interests or personal relationships that could have appeared to influence the work reported in this pape.

Credit author statement

Antonio Atienza-Márquez: Conceptualization, Methodology, Software, Validation, Formal analysis, Investigation, Writing – original draft, Writing – review & editing, Visualization. **Fernando Domínguez Muñoz**: Project administration, Funding acquisition, Conceptualization, Writing – review & editing, Supervision. **Francisco Fernández Hernández**: Project administration, Conceptualization. **José Manuel Cejudo López**: Supervision.

Declaration of competing interest

The authors declare that they have no known competing financial interests or personal relationships that could have appeared to influence the work reported in this paper.

Data availability

Data will be made available on request.

Acknowledgements

The authors acknowledge the Universidad de Málaga and "Programa Operativo FEDER Andalucía 2014–2020" the financial support of the contract UMA18-FEDERJA-247. The authors also gratefully acknowledge Mr. Pedro Quintero Jiménez, head of the energy services at Hospital Comarcal de la Axarquía, for providing data and helpful information concerning the system analysed.

Appendix

Appendix A.1. Monitored mains water temperature

Fig. A1 depicts the monthly averaged temperature of the mains water monitored between January 2020 and May 2021.

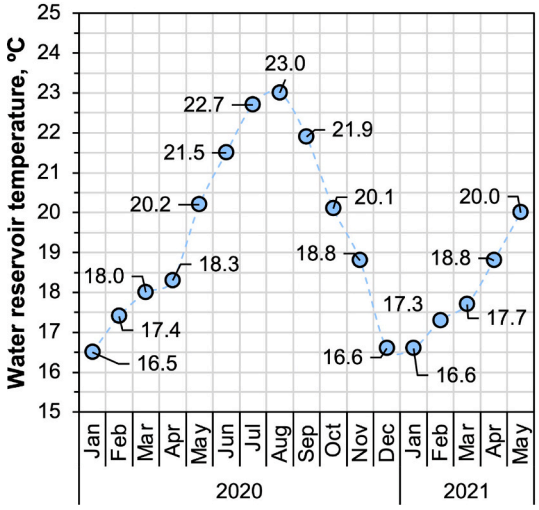

Fig. A.1. Variation of the temperature of the mains water.

Appendix A.2. Economics

The purchase equipment cost (*PEC*) of the main system components is estimated from the functions listed in Table A1. To update all the original costs obtained in year *y* to the reference year (i.e., 2020), the Chemical Engineering Plant Cost Index (CEPCI) [46] annual average composite values are used:

$$PEC_{2020} = PEC_y \times \left(\frac{CEPCI_{2020}}{CEPCI_y}\right) \tag{15}$$

The six-period electricity tariff schedules used in the simulation are depicted in Fig. A2. The net electricity consumed by the DHW installation ($W_{e,net}$) is calculated as follows:

$$W_{el,net} = W_{C,HP} + \sum W_P - W_{eq,AC} \tag{16}$$

The electricity consumed by the water-to-water heat pump ($W_{C,HP}$) is calculated from the following expression:

$$W_{C,HP} = \dot{Q}_{HP}/COP \tag{17}$$

where $\dot{Q}_{HP}$ represents the heat supplied by the heat pump. The coefficient of performance at part load operating conditions (COP) is calculated as follows [47]:

$$COP = [1 - 0.22 \times (1 - PLR)] \times COP_r \quad (18)$$

where the part load ratio (PLR) is defined as the ratio of the actual heat supplied by the heat pump to its rated heating capacity. The rated heating capacities and efficiencies (COP_r) used in the modelling are depicted in Table A2.

To calculate the parasitic consumption of circulation pumps (W_P) in Eq. (16), the following pressure drops are assumed: 195 kPa for the pump P1; 65 kPa for the pumps P2, P3, P4 and P5 (in case of installing a water-to-water heat pump); and 400 kPa for the recirculation pump P5. An EER of 3.0 W/W is assumed to calculate the equivalent electricity saving due to air-conditioning production ($W_{eq,AC}$).

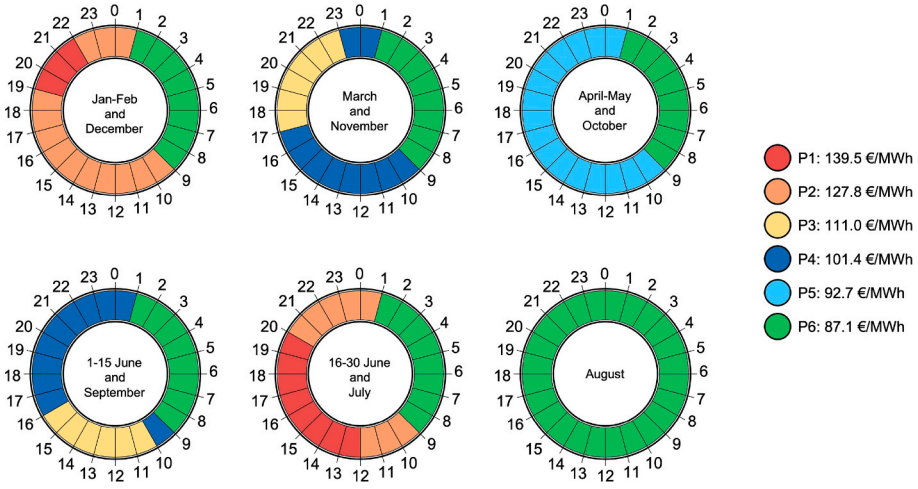

Fig. A.2. Six-period electricity tariff schedule used in the simulations based on rate 6.1TD in Spain.

Table A.1
Cost functions for the system components that integrate the hospital's domestic hot water installation.

System component	Equipment cost, €	Comment	Ref.
Solar collectors	$332 \times A_{[m^2]}$	Cost per net area flat plate solar thermal collectors based on the flat-plate model Vaillant VFK 135 VD. VAT included [a].	[48]
Thermal insulation	$f(U)_{[€/m]} \times L_{[m]}$	The cost of the thermal insultation of pipes relies on their length (L, in m) and heat transfer coefficient (U), which in turn is a function of the outer diameter of the pipe (D_o), the insulation thickness (δ) and its thermal conductivity ($k = 0.04$ W/(m^2·K)): $U^{-1} \cong D_o/(2\,k) \times ln(D_{is}/D_o)$. Fig. A3 shows the cost of the thermal insulation material (closed-cell elastomeric foam) for different U-values. Data obtained from vendor's quotation.	[49]
Water-to-water heat pump	$1,780 \times \dot{Q}^{0.573}_{HP,[kW]}$	Cost as a function of the heating capacity. Correlation developed by the authors from manufacturer's quotation (Carrier model 61 WG 020–090). VAT included [a].	[50]
Heat exchangers	$5,112 \times A^{0.650}_{[m^2]}$	Plate-and-frame heat exchangers made of stainless-steel [b]. To estimate the heat transfer area (A), the U-value is assumed 3 kW/(m^2·K).	[51]
Pumps	$952.0 \times W^{0.800}_{P,[kW]}$	Cost as a function of the power (in kW). The cost of the electric motor is assumed to be included [b].	[52]
Tanks	$5,294.6 \times V^{0.565}_{[m^3]}$	Cost for cylindrical steel thermal storage tank as a function of its volume (V, in m^3). The thermal insulation is assumed to be included in this cost.	[53]
Gas boiler	$170.0 \times \dot{Q}_{b,[kW]}$	Cost as a function of the rated heating capacity of the boiler ($\dot{Q}_b$, in kW).	[54]
Pasteuriser	$4,465.1 \times \dot{Q}^{0.346}_{PAST,[kW]}$	Cost as a function of the power of the pasteuriser (in kW). Correlation developed by the authors from manufacturer's quotation (Micronela model Legiopack LG01-014).	[55]

[a] Value added tax (VAT) applied to the recommended retail price (RRP): 21%.
[b] Currency conversion factor applied to the original cost function (from US dollars to Euros): 0.85 €/$.

Table A.2
Nameplate performance data of the water source heat pumps model 61WG-020-090 manufactured by Carrier [56].

Nameplate data	Model 61 WG (Carrier)								
	020	025	030	035	040	045	050	060	070
Heating capacity, kW	26	31	34	40	43	49	61	71	76
Coefficient of performance (COP)	2.96	2.96	2.86	2.93	2.88	2.96	2.98	3.04	2.99

Heating mode conditions: Evaporator entering/leaving water temperature 12/7 °C, condenser entering/leaving water temperature 55/65 °C.

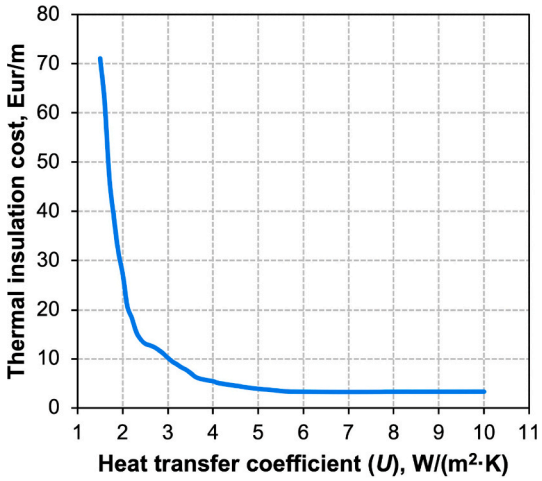

Fig. A.3. Cost of the thermal insulation (closed-cell elastomeric foam). in €/m-length, for different heat transfer coefficients of the hot water distribution network based on vendor's quotation [49].

References

[1] United Nations Environment Programme. Global status report for buildings and construction: towards a zero-emission, efficient and resilient buildings and construction sector. 2021, www.globalabc.org. [Accessed 20 October 2021].

[2] Economidou M, Todeschi V, Bertoldi P, D'Agostino D, Zangheri P, Castellazzi L. Review of 50 years of EU energy efficiency policies for buildings. Energy Build 2020;225:110322. https://doi.org/10.1016/J.Enbuild.2020.110322.

[3] D'Agostino D, Parker D, Epifani I, Crawley D, Lawrie L. How will future climate impact the design and performance of nearly zero energy buildings (NZEBs)? Energy 2022;240:122479. https://doi.org/10.1016/J.Energy.2021.122479.

[4] Moran P, O'Connell J, Goggins J. Sustainable energy efficiency retrofits as residenial buildings move towards nearly zero energy building (NZEB) standards. Energy Build 2020;211:109816. https://doi.org/10.1016/J.Enbuild.2020.109816.

[5] Santos-Herrero JM, Lopez-Guede JM, Flores-Abascal I. Modeling, simulation and control tools for nZEB: a state-of-the-art review. Renew Sustain Energy Rev 2021; 142:110851. https://doi.org/10.1016/J.Rser.2021.110851.

[6] Li DHW, Yang L, Lam JC. Zero energy buildings and sustainable development implications – a review. Energy 2013;54:1–10. https://doi.org/10.1016/J.Energy.2013.01.070.

[7] Belussi L, Barozzi B, Bellazzi A, Danza L, Devitofrancesco A, Fanciulli C, Ghellere M, Guazzi G, Meroni I, Salamone F, Scamoni F, Scrosati C. A review of performance of zero energy buildings and energy efficiency solutions. J Build Eng 2019;25:100772. https://doi.org/10.1016/J.Jobe.2019.100772.

[8] Dehwah AHA, Krarti M. Energy performance of integrated adaptive envelope systems for residential buildings. Energy 2021;233:121165. https://doi.org/10.1016/J.Energy.2021.121165.

[9] Duran Ö, Lomas KJ. Retrofitting post-war office buildings: interventions for energy efficiency, improved comfort, productivity and cost reduction. J Build Eng 2021; 42:102746. https://doi.org/10.1016/J.Jobe.2021.102746.

[10] Gil-Baez M, Barrios-Padura Á, Molina-Huelva M, Chacartegui R. Natural ventilation systems in 21st-century for near zero energy school buildings. Energy 2017;137:1186–200. https://doi.org/10.1016/J.Energy.2017.05.188.

[11] Salem R, Bahadori-Jahromi A, Mylona A, Godfrey P, Cook D. Energy performance and cost analysis for the nZEB retrofit of a typical UK hotel. J Build Eng 2020;31: 101403. https://doi.org/10.1016/J.Jobe.2020.101403.

[12] Buonomano A, Calise F, Ferruzzi G, Palombo A. Dynamic energy performance analysis: case study for energy efficiency retrofits of hospital buildings. Energy 2014;78:555–72. https://doi.org/10.1016/J.Energy.2014.10.042.

[13] González González A, García-Sanz-Calcedo J, Salgado DR. A quantitative analysis of final energy consumption in hospitals in Spain. Sustain Cities Soc 2018;36: 169–75. https://doi.org/10.1016/J.Scs.2017.10.029.

[14] Bawaneh K, Ghazi Nezami F, Rasheduzzaman M, Deken B. Energy consumption analysis and characterization of healthcare facilities in the United States. Energies 2019;12:3775. https://doi.org/10.3390/En12193775.

[15] Abd Rahman NM, Lim CH, Fazlizan A. Optimizing the energy saving potential of public hospital through a systematic approach for green building certification in Malaysia. J Build Eng 2021;43:103088. https://doi.org/10.1016/J.Jobe.2021.103088.

[16] García-Sanz-Calcedo J, Gómez-Chaparro M, Sanchez-Barroso G. Electrical and thermal energy in private hospitals: consumption indicators focused on healthcare activity. Sustain Cities Soc 2019;47:101482. https://doi.org/10.1016/J.Scs.2019.101482.

[17] Teke A, Timur O. Overview of energy savings and efficiency strategies at the hospitals. Int. J. Soc. Manag. Econ. Bus. Eng. 2014;8:257–63. https://doi.org/10.5281/Zenodo.1090536.

[18] Teke A, Timur O. Assessing the energy efficiency improvement potentials of HVAC systems considering economic and environmental aspects at the hospitals. Renew Sustain Energy Rev 2014;33:224–35. https://doi.org/10.1016/J.Rser.2014.02.002.

[19] Yuan F, Yao R, Sadrizadeh S, Li B, Cao G, Zhang S, Zhou S, Liu H, Bogdan A, Croitoru C, Meliko AK, Short CA, Li B. Thermal comfort in hospital buildings – a literature review. J Build Eng 2021:103463. https://doi.org/10.1016/J.Jobe.2021.103463.

[20] Heras Celemín M del R, Ferrer Tévar JA, Seco Calvo O, Rodríguez G, Rodríguez J, Fernández Artime R, García-Luengo Manchado F, Escobar López GJ, Orduna Onco FJ. Visión de la eficiencia energética en el sector hospitalario. 2015.

[21] Fuentes E, Arce L, Salom J. A review of domestic hot water consumption profiles for application in systems and buildings energy performance analysis. Renew Sustain Energy Rev 2018;81:1530–47. https://doi.org/10.1016/J.Rser.2017.05.229.

[22] Shen C, Zhao K, Ge J, Zhou Q. Analysis of building energy consumption in a hospital in the hot summer and cold winter area. Energy Proc 2019;158:3735–40. https://doi.org/10.1016/J.Egypro.2019.01.883.

[23] Wang T, Li X, Liao P-C, Fang D. Building energy efficiency for public hospitals and healthcare facilities in China: barriers and drivers. Energy 2016;103:588–97. https://doi.org/10.1016/J.Energy.2016.03.039.

[24] Sánchez-Barroso G, González-Domínguez J, García-Sanz-Calcedo J. Potential savings in DHW facilities through the use of solar thermal energy in the hospitals of extremadura (Spain). Int J Environ Res Publ Health 2020;17:2658. https://doi.org/10.3390/Ijerph17082658.

[25] Trnsys vol. 18, (2017). https://sel.me.wisc.edu/trnsys/features/features.html (accessed 15 October 2021).

[26] EnergyPlus - Weather Data, (2019). https://energyplus.net/weather (accessed 10 December 2019).

[27] T*SOL – Valentin Software GmbH. n.d. https://valentin-software.com/en/products/tsol/. [Accessed 21 October 2021].

[28] Meister C, Beausoleil-Morrison I. Experimental and modelled performance of a building-scale solar thermal system with seasonal storage water tank. Sol Energy 2021;222:145–59. https://doi.org/10.1016/J.Solener.2021.05.025.

[29] Carretero-Ayuso MJ, García-Sanz-Calcedo J. Analytical study on design deficiencies in the envelope projects of healthcare buildings in Spain. Sustain Cities Soc 2018;42:139–47. https://doi.org/10.1016/J.Scs.2018.07.004.

[30] Hamburg A, Mikola A, Parts TM, Kalamees T. Heat loss due to domestic hot water pipes. Energies 2021;14:1–19. https://doi.org/10.3390/En14206446.

[31] Cholewa T, Siuta-Olcha A, Anasiewicz R. On the possibilities to increase energy efficiency of domestic hot water preparation systems in existing buildings – long term field research. J Clean Prod 2019;217:194–203. https://doi.org/10.1016/J.Jclepro.2019.01.138.

[32] Rahmatmand A, Vratonjic M, Sullivan PE. Energy and thermal comfort performance evaluation of thermostatic and electronic mixing valves used to provide domestic hot water of buildings. Energy Build 2020;212:109830. https://doi.org/10.1016/J.Enbuild.2020.109830.

[33] Meteonorm sotware. 2021. https://meteonorm.com/en/. [Accessed 15 October 2021].

[34] UNE-EN IEC 60751:2022. Industrial platinum resistance thermometers and platinum temperature sensors. 2022.

[35] Taylor BN, Kuyatt CE. NIST technical Note 1297 (1994 edition): Guidelines for evaluating and expressing the uncertainty of NIST measurement results. 1994.

[36] Garcia-Sanz-Calcedo J, Lopez-Rodriguez F, Yusaf T, Al-Kassir A. Analysis of the average annual consumption of water in the hospitals of extremadura (Spain). Energies 2017;10:479. https://doi.org/10.3390/En10040479.

[37] Ivanko D, Sørensen ÅL, Nord N. Selecting the model and influencing variables for DHW heat use prediction in hotels in Norway. Energy Build 2020;228:110441. https://doi.org/10.1016/J.Enbuild.2020.110441.
[38] Ivanko D, Walnum HT, Nord N. Development and analysis of hourly DHW heat use profiles in nursing homes in Norway. Energy Build 2020;222:110070. https://doi.org/10.1016/J.Enbuild.2020.110070.
[39] Hadengue B, Scheidegger A, Morgenroth E, Larsen TA. Modeling the water-energy nexus in households. Energy Build 2020;225:110262. https://doi.org/10.1016/J.Enbuild.2020.110262.
[40] Bujak J. Heat consumption for preparing domestic hot water in hospitals. Energy Build 2010;42:1047–55. https://doi.org/10.1016/J.Enbuild.2010.01.017.
[41] ASHRAE Guideline 14-2014. Measurement of energy, demand, and water savings. In: ASHRAE guidel. 14-2014, vol. 4; 2014. p. 1–150.
[42] Copiello S, Gabrielli L, Bonifaci P. Evaluation of energy retrofit in buildings under conditions of uncertainty: the prominence of the discount rate. Energy 2017;137:104–17. https://doi.org/10.1016/J.Energy.2017.06.159.
[43] Bejan A, Tsatsaronis G, Moran M. Thermal design and Optimization. Jonh Wiley & Sons, Inc.; 1996.
[44] Fujimori S, Krey V, van Vuuren D, Oshiro K, Sugiyama M, Chunark P, Limmeechokchai B, Mittal S, Nishiura O, Park C, Rajbhandari S, Silva Herran D, Tu TT, Zhao S, Ochi Y, Shukla PR, Masui T, Nguyen PVH, Cabardos A-M, Riahi K. A framework for national scenarios with varying emission reductions. Nat Clim Change 2021;11:472–80. https://doi.org/10.1038/S41558-021-01048-Z.
[45] Kim D, Yim T, Lee JY. Analytical study on changes in domestic hot water use caused by COVID-19 pandemic. Energy 2021;231:120915. https://doi.org/10.1016/J.Energy.2021.120915.
[46] The Chemical Engineering Plant Cost Index, (n.d.). https://www.chemengonline.com/site/plant-cost-index/(accessed 3 November 2021).
[47] Fuentes E, Waddicor DA, Salom J. Improvements in the characterization of the efficiency degradation of water-to-water heat pumps under cyclic conditions. Appl Energy 2016;179:778–89. https://doi.org/10.1016/J.Apenergy.2016.07.047.
[48] Vaillant Group Spain. Tariff, vol. 2021; 2021.
[49] Salvador Escoda SA. Aislamiento tubular flexible autoadhesivo Clase M1. Isocell®; 2021. https://www.salvadorescoda.com/tarifas/Aislamientos_Tarifa_PVP_SalvadorEscoda.pdf. [Accessed 1 September 2021].
[50] Carrier Spain. Heating, ventilation and air-conditioning. Prices 2018:33.
[51] Woods DR. Rules of Thumb in engineering practice. Wiley; 2007. https://doi.org/10.1002/9783527611119.
[52] Dorj P. Thermoeconomic analysis of a new Geothermal utilization CHP plant in Tsetserleg, Mongolia. University of Iceland; 2005.
[53] Sveinbjörnsson D, Linn P, Jensen L, Trier D, Ben Hassine I, Jobard X. D2.3 - large Storage Systems for DHC Networks. Fifth generation, low temperature, high exergy district heating and cooling networks. FLEXYNETS); 2017.
[54] Kozarcanin S, Hanna R, Staffell I, Gross R, Andresen GB. Impact of climate change on the cost-optimal mix of decentralised heat pump and gas boiler technologies in Europe. Energy Pol 2020;140:111386. https://doi.org/10.1016/J.Enpol.2020.111386.
[55] Micronela Legiopack. https://micronela.com/producto-legiopack/. [Accessed 18 October 2021].
[56] Carrier, AquaSnap® 61WG - Carrier heat pump. https://www.carrier.com/commercial/es/es/soluciones/bombas-de-calor-solo-calor/bombas-de-calor-agua-agua/61wg/#documents. [Accessed 30 July 2021].